Solar Physics
DOI: 10.1007/•••••-•••-•••-••••-•

Observations of Photospheric Vortical Motions During the Early Stage of Filament Eruption

Sajal Kumar Dhara[1] · **B. Ravindra**[1] · **Ravinder Kumar Banyal**[1,2]

© Springer ••••

Abstract Solar filaments/prominences exhibit rotational motion during different phases of their evolution from their formation to eruption. We have observed the rotational/vortical motion in the photosphere near the ends of ten filaments during their initial phase of eruption, at the onset of the fast rise phase. All the filaments were associated with active regions. The photospheric vortical motions we observed lasted for 4–20 minutes. In the vicinity of the conjugate ends of the filament the direction of rotation was opposite, except for two cases, where rotational motion was observed at only one end point. The sudden onset of a large photospheric vortex motion could have played a role in destabilizing the filament by transporting axial flux into the activated filament thereby increasing the outward magnetic pressure in it. The outward magnetic pressure may have pushed the filament/flux rope to the height where the torus instability criterion was satisfied, and hence it could have caused the filament instability and eruption.

Keywords: Prominences, Active; Active Regions, Velocity Field

arXiv:1410.3592v1 [astro-ph.SR] 14 Oct 2014

1. Introduction

Solar filaments are large structures which contain dense and cool ($\sim 10^4$ K) plasma embedded in the tenuous and hot corona. The filaments form above the neutral line of the photospheric magnetic field and survive for days to weeks (Martin, 1998). During their formation and evolution and prior to eruption they exhibit a variety of dynamical processes. Bidirectional flows of plasma were observed within quiet region filaments (Zirker, Engvold, and Martin, 1998) and in active region filaments (Alexander *et al.*, 2013). Oscillations were observed in erupting filaments (Bocchialini *et al.*, 2012). Rotational motion in erupting filaments/prominences have been observed (Panesar *et al.*, 2013).

[1] Indian Institute of Astrophysics, Bangalore 560034, India
email: sajal@iiap.res.in email: ravindra@iiap.res.in
[2] Institut für Astrophysik, Georg-August-Universitat Göttingen, Friedrich-Hund-Platz 1, 37077 Göttingen, Germany

Normally, the filament is considered to be situated in the lower part of a flux rope, where the dense matter is suspended in the magnetic cavity. In the CME structure, the dark cavity, below the bright leading edge, is considered to correspond to the twisted flux rope (Gibson *et al.*, 2006) and the filament is located below the dark cavity. Identification of cavities is difficult in active region filaments, as the cavity or flux ropes are low lying, compact structures in active regions. Hence, it is not trivial to identify the flux ropes in active regions prior to eruption. On many occasions the ends of filaments are considered as the ends of the lower part of a flux rope that has roots in the photosphere (van Ballegooijen, 2004; Kliem *et al.*, 2013).

During the rising phase of eruptions, filaments are sometimes observed to undergo a rotation about the vertical axis (see, *e.g.,* Zhou *et al.*, 2006; Green *et al.*, 2007; Liu *et al.*, 2009; Thompson, 2011). This kind of filament rotation is interpreted as a conversion of twist into writhe in a kink-unstable flux rope. The flux rope axis rotation is clockwise (as viewed from above) if it has right-handed twist and counter-clockwise if it has left-handed twist (see, *e.g.,* Rust and LaBonte, 2005; Green *et al.*, 2007; Wang, Muglach, and Kliem, 2009). Erupting prominences which are considered to be contained in magnetic flux ropes, very often develop into a helical-like structure (see, *e.g.,* Rust, 2003; Rust and LaBonte, 2005; Williams *et al.*, 2005; Liu *et al.*, 2007), which indicates the signature of a magnetohydrodynamics (MHD) kink instability of a twisted magnetic flux rope (Rust and LaBonte, 2005). In the twisted flux rope, the upward directed kink instability leads to the upward motion of the flux rope, which eventually turns into helical deformation and forms current sheets. The helical kink instability of a pre-existing flux rope can trigger solar eruptions (Török and Kliem, 2005). In the MHD instability, half the magnitude of the twist will be converted into writhe having the same sign as twist (Török *et al.*, 2014). The 'S' shaped stable filament reverses its shape to inverse 'S' while it is rising. During the rising phase, the shape of the erupting filament straightens out and later acquires the deformation of the axis in opposite direction suggesting the transition from 'S' to inverse 'S'. The possibility of this mechanism is confirmed in the numerical simulation of a kink–unstable flux rope by Török, Berger, and Kliem (2010). During the observation of such events the deformation of the shape can be seen as a rotation of the axis.

The filament/flux rope can face an another type of instability called "torus instability"(see, Kliem and Török, 2006; Zuccarello *et al.*, 2014). The toroidal current carrying flux rope experiences an outward directed self Lorentz force (also called a hoop force) which counteracts the external poloidal fields of the background magnetic fields (Chen, 1989; Titov and Démoulin, 1999). However, if the external poloidal field decreases faster with the radial distance than the self Lorentz force, then the flux rope can become unstable to the lateral expansion. A loss of equilibrium of the flux rope due to this effect can lead to its eruption.

Liggett and Zirin (1984) studied rotational motion in five non-eruptive prominences. In some events they reported only a part of the prominence rotating, while in the other the entire body was in rotation. They interpreted the rotation in terms of a twisting of the magnetic structure resulting from the

reconnection. *Atmospheric Imaging Assembly* (AIA; Lemen *et al.*, 2012) observations show that the feet of solar prominences exhibit coherent rotation for over three hours in the lower corona as the material is flowing along helical structures (Li *et al.*, 2012).

Su *et al.* (2012) reported two solar tornadoes during the formation of a quiet prominence. This tornado was observed for about two days. A systematic analysis of giant tornadoes by Wedemeyer *et al.* (2013) using AIA 171 Å images and high-resolution SST observations shows that giant tornadoes are an integral part of solar prominences. The tornadoes inject mass and twist into the filament spine until it becomes unstable and erupts. Su and van Ballegooijen (2013) also reported a quiescent filament eruption in which a part of the quiescent filament exhibits a strong clockwise rolling motion.

When a filament erupts non-radially, the top of its axis bends first to one side and propagates into sideways rolling motion, known as the *roll effect*, which results in a large scale twists in both legs of erupting filaments (see, *e.g.,* Bangert, Martin, and Berger, 2003; Filippov, Gopalswamy, and Lozhechkin, 2001; Panasenco *et al.*, 2011; Panasenco *et al.*, 2013). This rotational mass motion is observed to flow down as the structure of the filament rises to higher heights. If the observed sense of rotations was generated by the external forces at the legs of the erupting filament, then the sense of the twists in both legs is opposite to each other (Panasenco *et al.*, 2013). In the case of asymmetric eruption with respect to the polarity inversion line, the spine of the filament bends one side, which does not necessarily result in rotation in both legs of the filament, depending upon the instability (see, *e.g.,* Martin, 2003; Panasenco and Martin, 2008).

In the aforementioned cases, either the whole prominence was rotating around its vertical axis or photospheric vortex motions were observed at individual footpoints. Only in some cases a part of the prominence was observed to be rotating. Dhara, Ravindra, and Banyal (2014) have reported a photospheric vortex-like rotational motion at the ends of a filament during its eruption. In that observation they have reported only a single event in which the rotational motion started soon after the filament eruption was initiated and lasted for a few minutes.

In this paper, we extended this study to ten erupting active region filaments and searched for such rotational motions in and around the end points of these filaments. The rotational motions were studied by applying a local correlation tracking technique (LCT; November and Simon, 1988) to the photospheric dopplergram data. We looked for rotational (photospheric vortex) motion during the onset of the filament eruption. This paper is organized as follows. In Section 2 we describe the data used. The results are described in Section 3, and a brief summary and discussion are presented in Section 4.

2. Data Set

The AIA instrument onboard the *Solar Dynamics Observatory* (SDO; Pesnell, Thompson, and Chamberlin, 2012) provides imaging of the solar atmosphere in seven extreme ultraviolet (EUV) wavelength channels centered on specific lines. The temperature diagnostics of the EUV emissions cover the range from 6×10^4 to 2×10^7 K. It has

high image cadence (12 sec) and spatial resolution (0.6″/pixel). We obtained the chromospheric data observed in He II 304 Å wavelength for eight active regions (NOAA 11226, 11283, 11515, 11560, 11451, 11936, 12027 and 12035) associated with ten events. The full-disk EUV images of the Sun observed in 304 Å wavelength are obtained on 07 June 2011, 07 September 2011, 02 July 2012, 02 September 2012, 07 April 2012, 31 December 2013, 01 January 2014, 04 April 2014, and 15 April 2014, covering the ten events of filament eruption. The obtained data is corrected for the flat fielding, the bad pixels, and the spikes due to high energy particles. From these data sets the filament regions are extracted and tracked over time. This process provided data cubes showing the filament eruption for each of the events.

We also acquired the dopplergram data set from *Helioseismic and Magnetic Imager* (HMI; Scherrer *et al.*, 2012; Schou *et al.*, 2012) at a cadence of 45 sec. We obtained the dopplergram data for each event for about six hours covering the whole event of filament eruption. The obtained dopplergrams show several velocity patterns, and while looking for the small scale feature motions one has to remove the long term and very short term velocity patterns in sequence. To start with, we first removed the overall solar rotation from the dopplergram data. This has been done by using the following method. We first averaged the dopplergram data set without correcting for solar rotation. The gradient part of the rotational velocity pattern was extracted and subtracted from each of the dopplergram data. This procedure removed the overall solar rotational velocity patterns in the full-disk dopplergrams. Later, we interpolated these dopplergram data set to the AIA pixel resolution to match the spatial size of each pixel in the data set. Further, the dopplergrams were differentially rotated to the central meridian passing time of the active region. The usual 5-minute oscillations in the dopplergrams were suppressed by applying a subsonic filter with an upper cutoff velocity magnitude of 4 km s^{-1}. This corrected data set is used to determine the horizontal velocity of features near the footpoints of the filament and its surrounding regions at the photospheric level. This has been done by applying the LCT technique to the processed dopplergram data set as has been done in De Rosa and Toomre (2004) and Ravindra (2006).

Along with the aforesaid data sets, we also obtained the line-of-sight magnetograms from HMI for each events at a cadence of 45 sec for about a few hours before, during and after the eruption. We corrected the data set for the solar rotation in a similar way to the dopplergrams. The correction for the line-of-sight effect is made by multiplying $1/\cos\theta$, where θ is the heliocentric angle. We used these magnetograms to locate the filament position in the active region (AR).

3. Observations and Results

3.1. Events description

In this section we show the images only for four events. The remaining six events are shown in the appendix. The general appearance and location of filaments are depicted in Fig. 1 for four different events observed in He II 304 Å. In Fig. 1 their

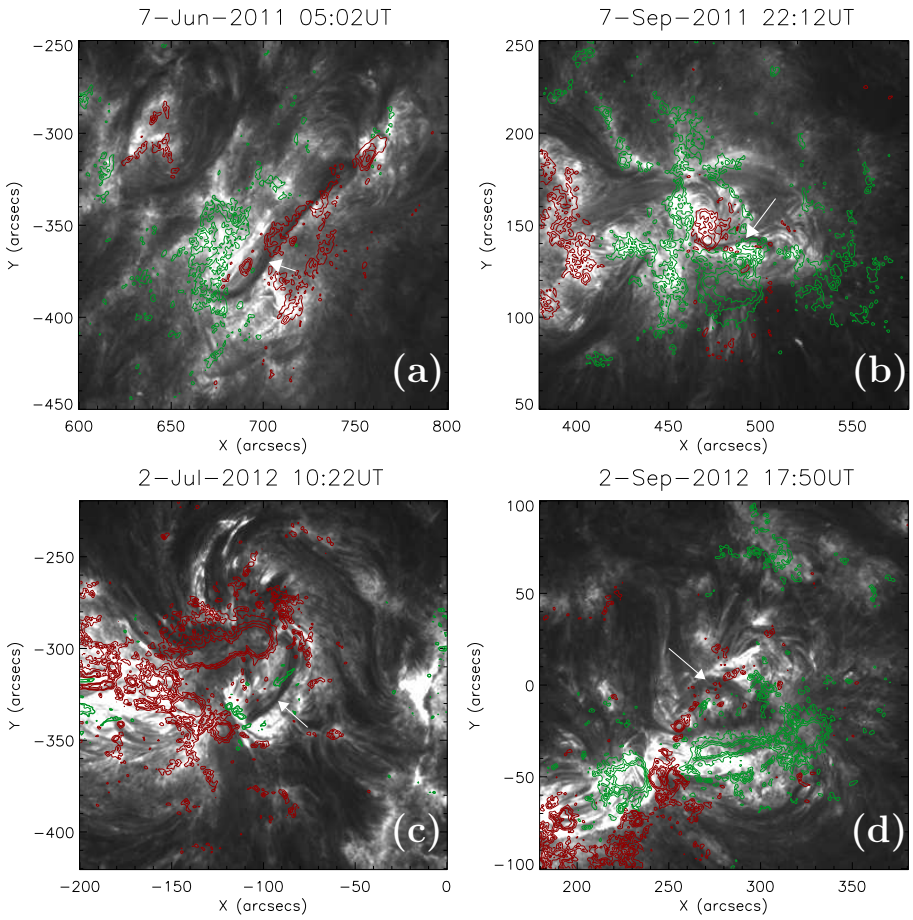

Figure 1. Filaments observed in SDO/AIA 304 Å channel in different active regions. The filament positions are shown by white arrows. Isocontours of the SDO/HMI magnetic strength values are overlaid on the images. The red and green contours represent the positive and negative polarities with magnetic field strength values of ± 150, 400, 600, and 900 G, respectively.

location is marked by an arrow. Isocontours of the magnetic field are overlaid upon the 304 Å images indicating that the filaments are associated with active regions. The location of these filaments on the Sun is given in Table 1. We used the events whose apparent central meridian longitude is less than 65° to avoid large projection effects on the observations. The filaments in EUV wavelengths appeared as dark features. The shape of the filament in Fig. 1b appears as 'S' in 304 Å wavelength before the activation and the other two filaments (Fig. 1c, d) appeared as small arcade shaped structures. While erupting, the filaments became dark over large areas and a large amount of material was ejected.

A time sequence of images showed that for events 1 (Fig. 1a) and 2 (Fig. 1b), both the eastern and the western footpoints of the filament were detached near simultaneously from the solar surface after activation, the filament reached some height, and eventually fell back to the solar surface. The movies for these failed eruption events are available on our ftp site[1]. In events 3 (Fig. 1c) and 4 (Fig. 1d), the eruptions took place in a different manner. The eastern footpoints of both filaments were detached first from the solar surface in association with brightening at the same location and later the bulk of filament material was seen escaping from the solar surface. As soon as the eastern footpoint of the filament detached, the filament expanded in its structure and started to rotate. The rotational motion was observed starting from ∼10:50 UT to ∼11:45 UT for event 3 and it was counter-clockwise as seen from above. A similar kind of rotational motion was observed for event 4, which lasted for about 9 minutes starting from ∼18:11 UT to ∼18:20 UT. The direction of rotation was observed to be clockwise. These movies are available on our ftp site[1]. The zoomed in versions of the erupting filaments are also shown in the same movies. This kind of rotation of the filament was not observed for events 1 and 2. The movies for events 5–10 are also available on the same ftp site[1].

By examining the time series of 304 Å images for each event we determined the filament activation time (see Table 1). The projected average velocities of the erupting filaments also shown in Table 1, are computed by tracking the features of the erupting filaments within the field-of-view during their eruptions.

3.2. Flows in and around the filament footpoints

In order to measure photospheric flows in and around sunspot regions and filaments, we applied the Fourier local correlation tracking (FLCT; Welsch *et al.*, 2004) technique to dopplergrams. Selecting the two parameters such as the time difference between the two images and the size of the Gaussian apodizing window functions are crucial in finding the velocity vectors. We used the dopplergram images which are 3 minutes apart and the apodizing window width of $9''$ as a window function. The obtained velocity vectors are averaged over ∼1.5 hours to examine the long term flows in and around the active regions. Figure 2 shows the long lived flows for the first four events listed in Table 1. The contours of the filament are overlaid upon the velocity map to mark the location of the filament and its end points. Filament contours are extracted from the 304 Å images for each event. The boxed regions 1 and 2 show the eastern and western footpoints of the filament regions, respectively. Around the sunspots outward flows are observed. At filament end points either converging motions or large scale outflows were observed.

[1]Movies generated from SDO/AIA 304 Å images of the filament eruptions associated with active region NOAA 11226, 11283, 11515, and 11560 discussed in this paper are available on our ftp site (ftp://ftp.iiap.res.in/sajal/). The movies are named according to the date of observations of the events. The movies for events 5–10 discussed in this paper are also available on the same ftp site.

Table 1. Event number is shown in the first column of the table. The date of observations, filament location on the Sun, associated active region number, filament activation time (AT), GOES class of the associated flare, average velocities and fast rise time (FRT) of the erupting filaments are given in the next seven columns. The duration and type of rotational motions observed for each events are listed in the final four columns. In the tenth and twelfth columns of the table, the abbreviation AC corresponds to anti-clockwise and C corresponds to clockwise direction of rotational motions.

Event No.	Date	Filament Location	AR NOAA	AT (UT)	GOES Flares	Velocity (km s^{-1})	FRT (UT)	Rotational Motion Observed in Eastern footpoint Duration (UT)	Type	Western footpoint Duration (UT)	Type
1	07–Jun–2011	∼S22W64	11226	∼05:56UT	M2.5	181.7±7.1	∼06:14	05:55:26–06:02:11	AC	06:08:56–06:23:11	C
2	07–Sep–2011	∼N14W30	11283	∼22:08UT	X1.8	193.9±1.9	∼22:30	22:13:22–22:17:07	C	22:17:52–22:24:37	AC
3	02–Jul–2012	∼S17E03	11515	∼10:31UT	M5.6	90.9±0.8	∼10:43	10:34:25–10:46:25	AC	–	–
4	02–Sep–2012	∼N03W18	11560	∼17:52UT	C5.5	42.9±0.4	∼18:03	18:08:51–18:14:51	C	17:56:51–18:04:21	AC
5	07–Apr–2012	∼N18W30	11451	∼17:45UT	C2.4	39.4±1.6	∼17:58	17:45:34–17:52:19	AC	17:45:34–17:56:04	C
6	31–Dec–2013	∼S16W32	11936	∼21:26UT	M6.4	149.0±2.7	∼21:46	21:37:54–21:43:54	AC	21:16:54–21:36:24	C
7	01–Jan–2014	∼S16W46	11936	∼16:18UT	–	11.4±0.3	∼16:23	16:09:24–16:18:24	AC	16:19:09–16:23:39	C
8	01–Jan–2014	∼S16W48	11936	∼18:21UT	M9.9	73.4±2.9	∼18:40	18:14:39–18:23:39	AC	18:10:09–18:25:09	C
9	04–Apr–2014	∼N13E15	12027	∼13:28UT	C8.3	109.5±3.0	∼13:33	13:28:17–13:39:32	C	13:46:17–13:58:17	AC
10	15–Apr–2014	∼S18E23	12035	∼17:33UT	C7.3	44.6±1.4	∼17:51	17:31:19–17:44:49	AC	–	–

In the boxed regions, during the early stage of the filament eruption the situation was different. The flow fields in the boxed regions of Fig. 2 showed rotational motions for a few minutes. These velocity flow fields were obtained from time sequence of images without averaging the velocity maps. Figure 3 shows the temporal sequence of flow field in the footpoints of the filaments which erupted on 07 June 2011 (event 1). We observed counter-clockwise rotation at the eastern footpoint and clockwise rotation at the western footpoint. The rotational pattern persisted for 7 and 15 minutes in the eastern and western footpoints, respectively.

The 07 September 2011 event showed clockwise rotation in the eastern footpoint and anti-clockwise rotation in the western footpoint. These rotational motions are shown in Fig. 4. But only in the wastern footpoint of the erupting filament an anti-clockwise rotational motion was observed on 02 July 2012 event(event 3, Fig. 5). The western footpoint did not show any rotational motion during the filament eruption in this event. This footpoint was located close to the penumbral portion of the sunspot region. Similarly, the 02 September 2012 event showed a clockwise rotation in the eastern footpoint and anti-clockwise rotation in the western footpoint of the filament(event 4, Fig. 6). In all the events the filament footpoint was located at the periphery of the rotation center. The rotation lasted for 4–20 minutes in each of these events.

The observed rotational motion is not simultaneous in both ends of the filament. There is about one to ten minute time difference between the ending of the rotational motion in one of the footpoints and starting in another footpoint of the filament. Table 1 provides the starting and ending times of the rotational motions seen in the ends of the filaments for all the events. The duration of the rotational motions in any one footpoint is about 4–20 minutes. In each of these events, the fast rise of the filament was observed either during or after the rotational motion observed. Table 1 provides the direction of rotation in each of the footpoint. It should be noted here that the direction of rotation is opposite in each filament end points. In two events (3 and 10), one end of the filament was located in the sunspot penumbral region where we did not find any rotational motion. We did not see any correlation between the speed of the filament eruption and duration of rotation. The average rotational speed at the footpoint of the filament is about 0.2 km s^{-1}, or about 6 deg hr^{-1}.

We have also observed rotational motions at other locations in the active region during the onset of the filament eruption. But the sizes of those rotating regions are significantly smaller compared to the reported one and they survived for 2–3 minutes only. One such rotational motion can be seen in Fig. 3 (top-right) at ($70''$, $50''$) pixel location. The rotational region is small, $10''$ in size. But those seen close to the filament ends are of supergranular size. The filaments are considered as the lower ends of the flux ropes which are embedded in the cavities of helical fields (Mackay *et al.*, 2010; Guo *et al.*, 2010). The 193 Å movies of four regions (events no. 1–4) provided on the ftp site[1] show the erupting filament and

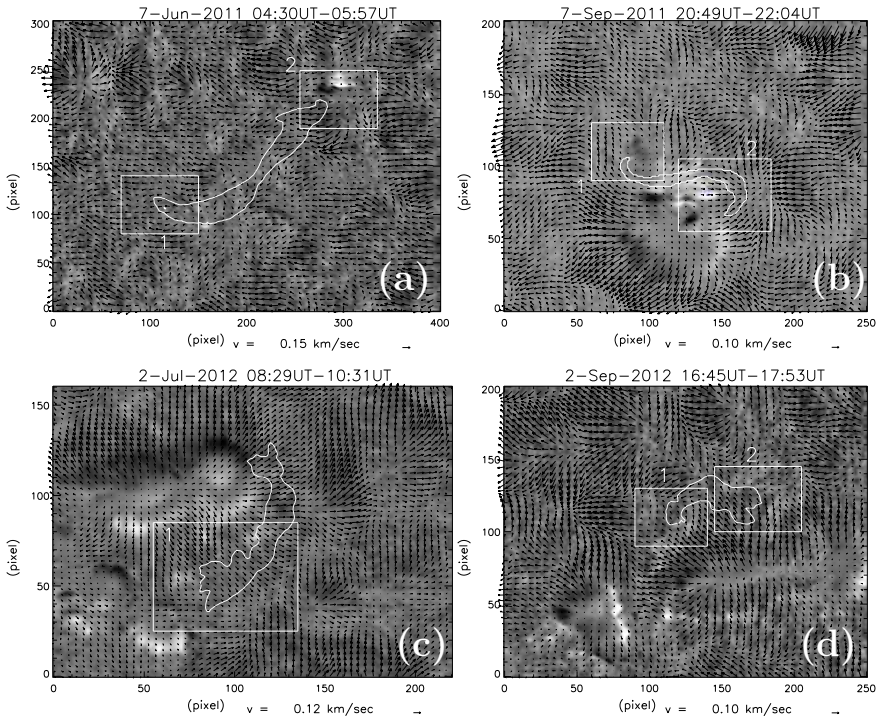

Figure 2. Averaged horizontal velocity vectors (arrows) are overlaid upon the averaged dopplergram for the first to fourth events. The black, white, and gray regions in the averaged dopplergram represent, respectively, the line-of-sight doppler velocities with upflow, downflow, and close to zero velocity. The averaging time interval is given above each figure. The white contours of the filaments, extracted from the 304 Å SDO/AIA images are overlaid upon the averaged dopplergram. The boxed regions 1 and 2 show the location of the eastern and western footpoints of the filament, respectively.

the evolving bright flux rope. The general view of the flux rope evolution can be obtained through Cheng *et al.* (2014).

4. Summary and Discussion

We have analyzed ten filament eruptions from eight different active regions at different times during Solar Cycle 24. Nine out of the ten filament eruption events were followed by a flare. In one event, the filament destabilized a couple of hours before the large flare (event no. 7). During the initial stages of filament eruption, in eight events, if one type of rotational motion was observed in one

[1]Movies generated from SDO/AIA 193 Å images of the filament eruptions associated with active region NOAA 11226, 11283, 11515 and 11560 discussed in this paper are available on our web site (ftp://ftp.iiap.res.in/sajal/). The movies are named according to the date of observations of the events.

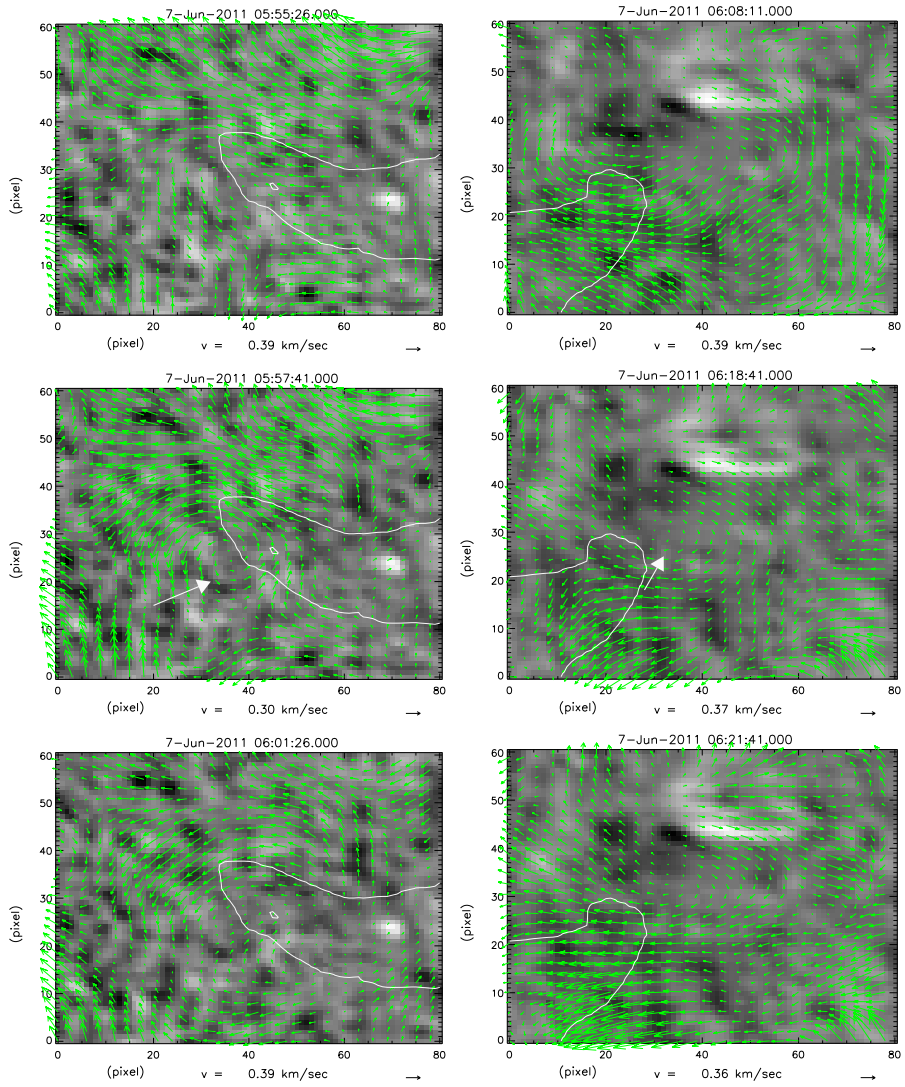

Figure 3. The temporal evolution of rotational velocity pattern observed for event 1. The left column corresponds to location 1 and right column for location 2 of Fig. 2(a). The filament contour extracted from the 304 Å image closest in time is overlaid upon the dopplergram. The rotation regions are indicated by a white arrow. The date and time of the computed velocity is shown above each map. The size of the arrow below each map represents the magnitude of velocity.

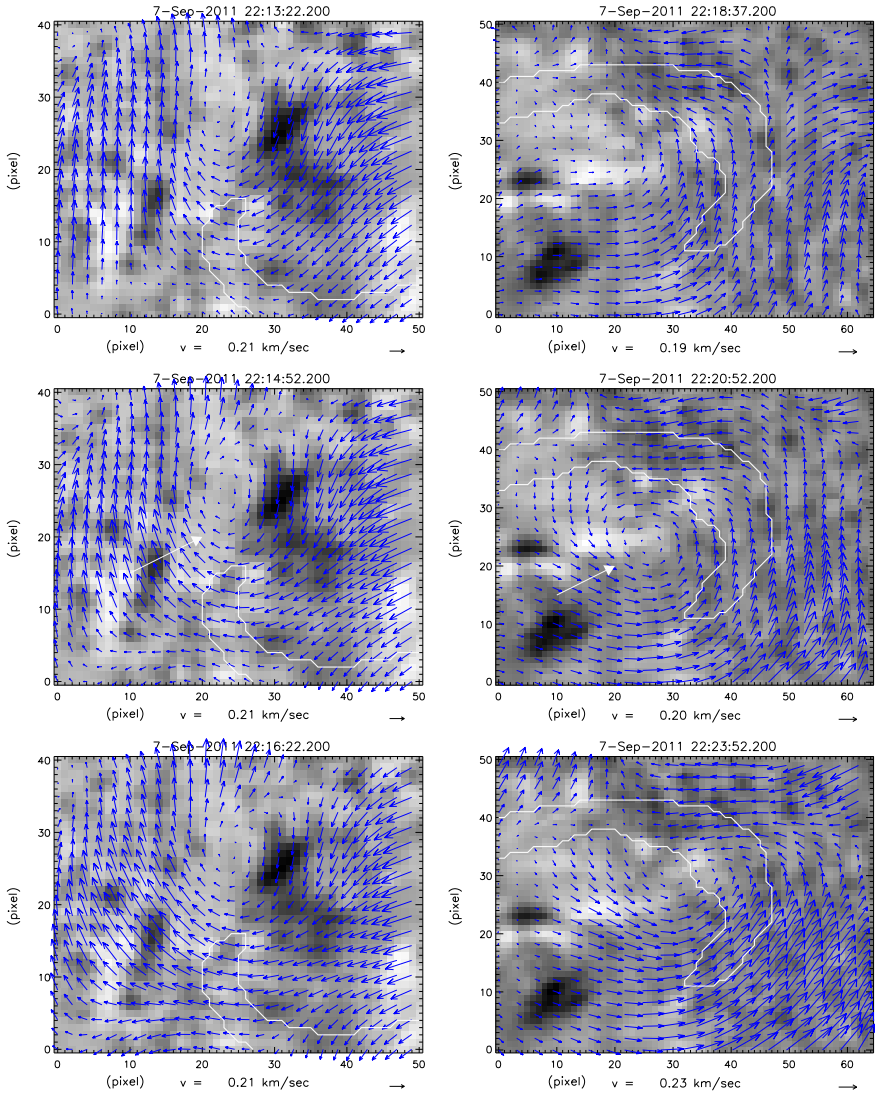

Figure 4. Same as Fig. 3, but for event 2.

end of the filament, the opposite direction of rotational motion was observed in the other end of the filament. In two events (3 and 10) the rotational motion was observed only in one end of the filament. The rotational motions persisted for about 4–20 minutes and the rate of rotation was about 6° hr^{-1}. The observed rotational motions in both ends of the filament are not simultaneous. There is a few minutes difference between the ending of the rotational motion at one end of the filament and starting of the rotational motion in the vicinity of another end

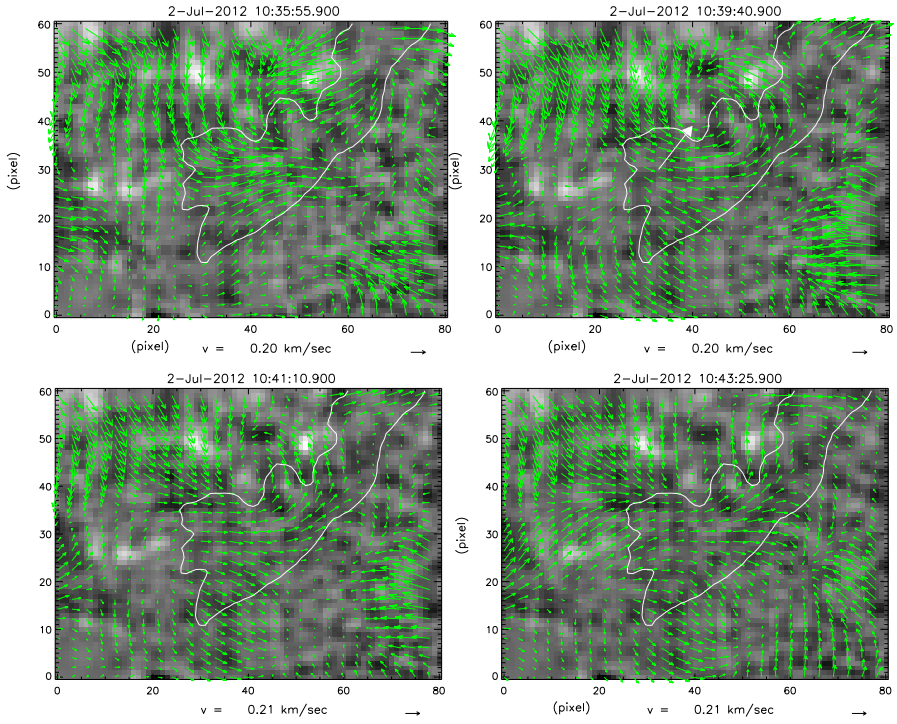

Figure 5. Same as Fig. 3, but for the region 1 of event 3.

of the filament. In all these events, the fast rising phase initiated either during the rotational motions or after they have ceased.

The filament destabilization and subsequent eruption may have been initiated due to several reasons such as a kink-mode instability in twisted magnetic fields (Sakurai, 1976), the magnetic reconnection at low level (Contarino *et al.*, 2003), flux cancelation at the photosphere (see, *e.g.,* Amari *et al.*, 2003) etc. Once the filament starts to erupt, it expands axially towards higher heights. As it rises, the local external pressure is smaller compared to the previous location of the filament. Because of the pressure difference, the top portion of the filament expands radially, thereby inducing a torque imbalance between the expanded portion and undisturbed portion of the filament (Parker, 1974; Jockers, 1978). The consequence of the radial expansion of the filament is a rotational motion in the expanded portion of the filament. This can happen by transferring the twist from the undisturbed portion to the expanded portion. The effect of the transfer of twist from the undisturbed portion to the expanded portion can lead to the rotation in the legs of the filaments, which could extend from the corona to the chromosphere. In this case two footpoints of the filament should exhibit oppositely directed motions (Jockers, 1978). The plasma inside the filament will also rotate with the flux rope. However, this cannot cause the observed rotational motions of the plasma in the photosphere where the plasma beta is large.

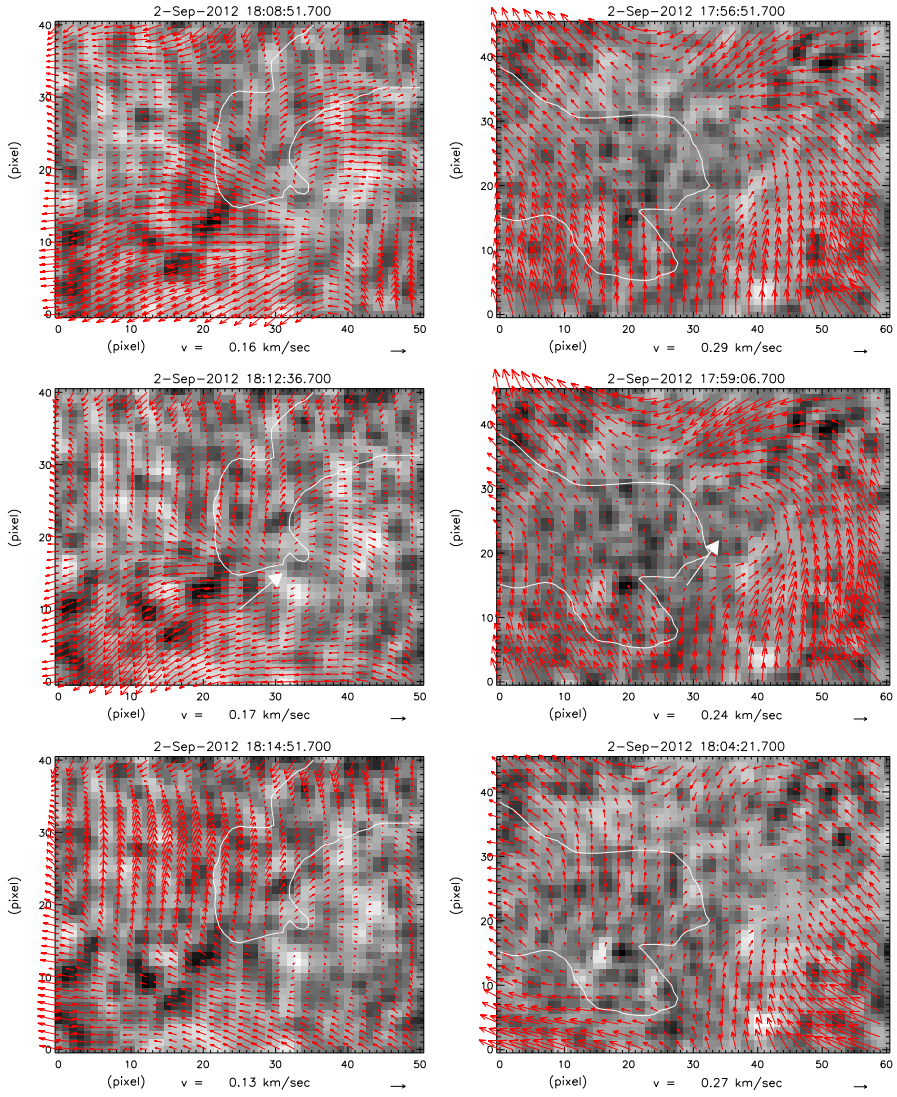

Figure 6. Same as Fig. 2, but for event 4.

Alternatively, the bending of the top portion of the erupting filament can induce the rotation of the legs. Martin (2003) and Panasenco and Martin (2008) have observed a bending motion of the top portion of the erupting prominence and subsequently observed an oppositely twisting motion in two legs. They name this phenomenon the "roll effect". Similarly, Panasenco *et al.* (2013) mention that the non-radially erupting prominence first exhibits a bending motion of the top of the prominence and later an oppositely directed rolling motion propagates into its legs. In this mechanism the plasma inside the flux rope can rotate with

the magnetic field and the rotational motion may not reach the photosphere as the torque and force required for the photospheric plasma to rotate is probably much larger than this.

The observed photospheric rotational motion near the ends of the filament could possibly be resulting from the photospheric or subphotospheric shearing flows. We observed that the fast rise of the filament was initiated during/after the vortical motion of the plasma had set in. We have also observed vortical flows offset from the ends of the filament. However, their lifetime is too short and their size is about $10''$, which is much smaller than the ones observed near the filament ends. The spatial correlation between the observed end points of the filament and the location of the rotational motion, and the temporal coincidence of the rotational motions with the filament eruption time in ten events suggest us that the observed rotational motion is not randomly occurring in the vertices of the supergranulation (Innes *et al.*, 2009).

When the filament starts to erupt, it expands axially towards higher heights. The immediate consequence of the deformation of the axial component of the magnetic field in the flux rope is the launch of shear Alfvèn waves by shearing its footpoints (by the Lorentz force) that in turn carry the axial component of the flux into the expanded portion of the flux rope (Manchester *et al.*, 2004). The increase in the axial flux in the flux rope will increase the magnetic pressure. The tendency of the outward directed magnetic pressure will push the flux rope slowly to higher heights. Once the top of the flux rope reaches a critical height where the torus instability criteria are satisfied then the flux rope becomes unstable and eventually it will erupt (Kliem and Török, 2006).

Another possibility is that, if there is an emergence of a poloidal flux, it results in a rotation of the footpoints. The injection of the poloidal flux into the flux rope, will increase the magnitude of the outward Lorentz self force (hoop force). This will push the flux rope slowly to critical height where the external poloidal flux is decreasing faster than the decrease of the hoop force. This condition will again lead to the torus instability and in that condition the flux rope is no longer in equilibrium scenario and eventually it erupts. But the generation and emergence of the poloidal field is very unlikely and there is no observational support to this [*see also* Chen and Kunkel, 2010].

Martin (2003) and Panasenco *et al.* (2011) reported that there is a correlation between the direction of the rolling motion observed in the erupting filament and the chirality of the filament. The observed directions of rotation in both legs of the prominence are opposite to each other. In future, we plan to study the rotation in the footpoints of a large number of erupting filaments using a spectroscopic technique both in the photosphere and chromosphere simultaneously along with their sign of chirality using vector magnetic field measurements. This may provide a vital clue to the origin of the rotational motion near the ends of the erupting filaments.

Acknowledgements We thank the referee for insightful comments which helped us to improve the content in the manuscript. The AIA data used here are the courtesy of NASA/SDO and AIA consortium. SDO/HMI is a joint effort of many teams and individuals to whom we are greatly indebted for providing the data.

Appendix

The filament locations in He II 304 Å SDO/AIA channel for events 5–10 are displayed in Figs. 7 to 12(a), respectively. The position of the filament on an averaged dopplergram (greyscale) and averaged horizontal flow map (arrows) is shown by overlying the contours of the filament extracted from 304 Å images. These are shown in Figs. 7 to 12(b), respectively. The observed rotational motions at the ends of the filament footpoints for all the events are also shown in bottom-left(c) and bottom-right(d) rows in Figs. 7 to 12. The date and time of the observations, the filament location on the Sun, associated active region number, the filament activation time, importance of the associated flare, and the velocities of the erupting filaments are given in Table 1. The starting and ending time and the type of the rotational motions seen at both ends of the filaments for all events are also given in the same table.

The filament in event 5 is a long one, associated with two active regions. One of its ends is located in AR 11451 and the other end is in AR 11450. Before the filament eruption, bidirectional flows were observed in the filament. There were three filament eruptions observed in AR 11936(events 6–8). Event 6 was observed on 31 December 2013. The other two events were observed on 01 January 2014. On 31 December 2013 only one filament existed in the active region and before the eruption this filament bifurcated into two halves. The right-side half erupted and the left-side one did not erupt. Later, again a filament formed in the same region and the bifurcation disappeared. Event 7 also occurred in the same active region, but the filament was located North of the 31 December 2013 event. This was a failed filament eruption. Event 8 also occurred on the same day, a few hours after event 7. The erupting filament was the same as the one which erupted on 31 December 2013. Unlike the 31st December event, however, here the whole filament was activated with no bifurcation. But it was a failed eruption. In event 9, AR 12027 was surrounded by filaments in all directions. It was not a single filament, in fact it was a group of 3–4 segmented filaments. On 04 April 2014 the North-East portion of the filament erupted (event 9). Before the eruption a large scale mass flow was observed inside the filament. Event 10 occurred in AR 12035. The filament was hard to see before the eruption in the active region. But during the filament activation a cusp shaped filament was observed in the active region. This filament erupted completely during a C7.3 class flare.

References

Alexander, C.E., Walsh, R.W., Régnier, S., Cirtain, J., Winebarger, A.R., Golub, L., Kobayashi, K., Platt, S., Mitchell, N., Korreck, K., DePontieu, B., DeForest, C., Weber, M., Title, A., Kuzin, S.: 2013, Anti-parallel EUV Flows Observed along Active Region Filament Threads with Hi-C. *Astrophys. J. Lett.* **775**, L32. DOI. ADS.

Amari, T., Luciani, J.F., Aly, J.J., Mikic, Z., Linker, J.: 2003, Coronal Mass Ejection: Initiation, Magnetic Helicity, and Flux Ropes. II. Turbulent Diffusion-driven Evolution. *Astrophys. J.* **595**, 1231. DOI. ADS.

Bangert, P.D., Martin, S.F., Berger, M.A.: 2003, Solar Coronal Magnetic Filaments: The Roll Effect in Erupting Prominences. In: *AAS/Solar Physics Division Meeting #34, Bulletin of the American Astronomical Society* **35**, 815. ADS.

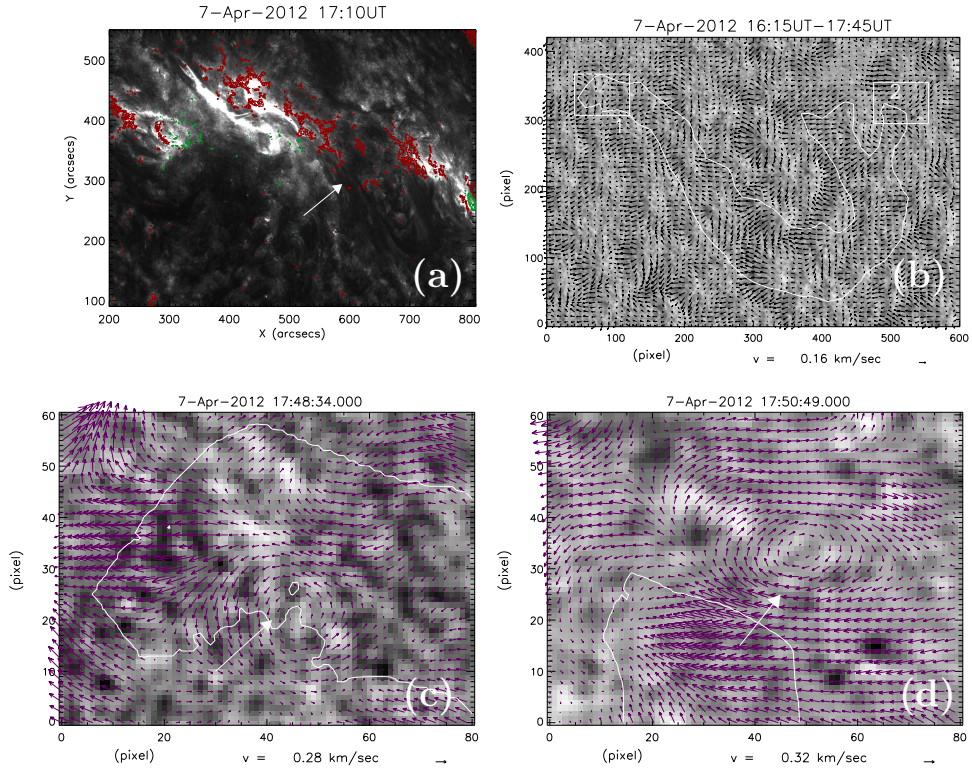

Figure 7. (a) The filament observed in SDO/AIA 304 Å channel for event 5 is indicated by a white arrow. Magnetic field isocontours from SHO/HMI overlaid on the 304 Å image. The red and green contours represent the positive and negative polarities with magnetic field strength values of ± 150, 400, 600 and 900 G, respectively. (b) Averaged horizontal velocity vectors shown in arrows are overlaid upon an averaged dopplergram. The duration of the averaging time is given above the panel. The contour of the filament, extracted from the 304 Å image is also shown. The boxed regions 1 and 2 show the location of the eastern and western ends of the filament respectively. (c, d) Rotational velocity pattern observed for this event. (c) image corresponds to location 1 and (d) to location 2 in (b).

Bocchialini, K., Koutchmy, S., Solomon, J., Tavabi, E.: 2012, Homologous flares inducing EUV filament oscillations with subsequent eruption. In: Faurobert, M., Fang, C., Corbard, T. (eds.) *EAS Publ. Ser.* **55**, 335. DOI. ADS.

Chen, J.: 1989, Effects of toroidal forces in current loops embedded in a background plasma. *Astrophys. J.* **338**, 453. DOI. ADS.

Chen, J., Kunkel, V.: 2010, Temporal and Physical Connection Between Coronal Mass Ejections and Flares. *Astrophys. J.* **717**, 1105. DOI. ADS.

Cheng, X., Ding, M.D., Guo, Y., Zhang, J., Vourlidas, A., Liu, Y.D., Olmedo, O., Sun, J.Q., Li, C.: 2014, Tracking the Evolution of a Coherent Magnetic Flux Rope Continuously from the Inner to the Outer Corona. *Astrophys. J.* **780**, 28. DOI. ADS.

Contarino, L., Romano, P., Yurchyshyn, V.B., Zuccarello, F.: 2003, Themis, BBSO, MDI and trace observations of a filament eruption. *Solar Phys.* **216**, 173. DOI. ADS.

De Rosa, M.L., Toomre, J.: 2004, Evolution of Solar Supergranulation. *Astrophys. J.* **616**, 1242. DOI. ADS.

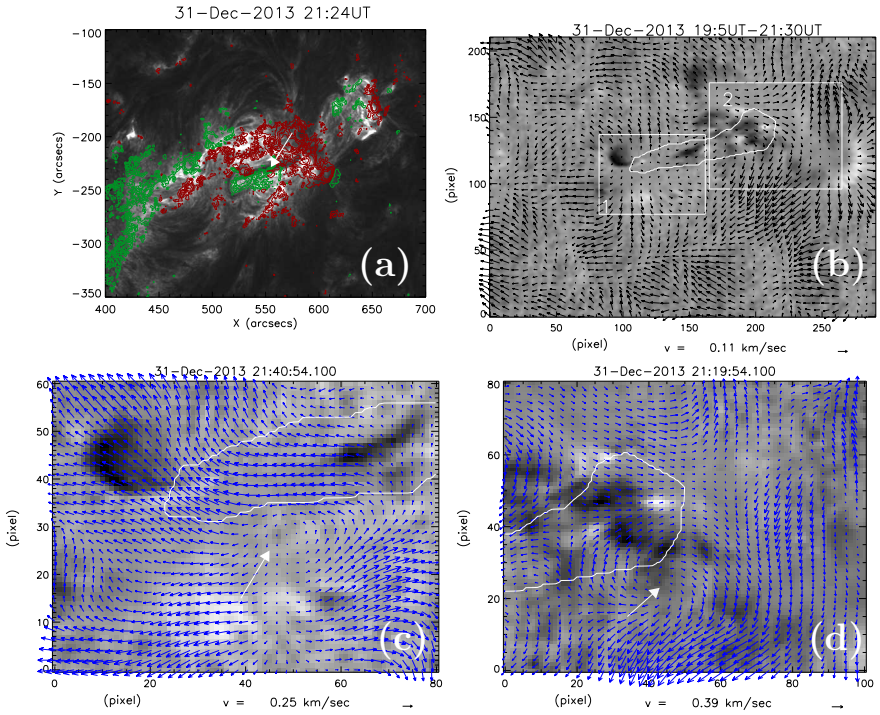

Figure 8. Same as Fig. 7, but for event 6.

Dhara, S.K., Ravindra, B., Banyal, R.K.: 2014, Filament eruption in association with rotational motion near the filament footpoints. *New Astron.* **26**, 86. DOI. ADS.

Filippov, B.P., Gopalswamy, N., Lozhechkin, A.V.: 2001, Non-radial motion of eruptive filaments. *Solar Phys.* **203**, 119. ADS.

Gibson, S.E., Foster, D., Burkepile, J., de Toma, G., Stanger, A.: 2006, The Calm before the Storm: The Link between Quiescent Cavities and Coronal Mass Ejections. *Astrophys. J.* **641**, 590. DOI. ADS.

Green, L.M., Kliem, B., Török, T., van Driel-Gesztelyi, L., Attrill, G.D.R.: 2007, Transient Coronal Sigmoids and Rotating Erupting Flux Ropes. *Solar Phys.* **246**, 365. DOI. ADS.

Guo, Y., Schmieder, B., Démoulin, P., Wiegelmann, T., Aulanier, G., Török, T., Bommier, V.: 2010, Coexisting Flux Rope and Dipped Arcade Sections Along One Solar Filament. *Astrophys. J.* **714**, 343. DOI. ADS.

Innes, D.E., Genetelli, A., Attie, R., Potts, H.E.: 2009, Quiet Sun mini-coronal mass ejections activated by supergranular flows. *Astron. Astrophys.* **495**, 319. DOI. ADS.

Jockers, K.: 1978, Transport of twist in force-free magnetic flux tubes. *Astrophys. J.* **220**, 1133. DOI. ADS.

Kliem, B., Török, T.: 2006, Torus Instability. *Physical Review Letters* **96**(25), 255002. DOI. ADS.

Kliem, B., Su, Y.N., van Ballegooijen, A.A., DeLuca, E.E.: 2013, Magnetohydrodynamic Modeling of the Solar Eruption on 2010 April 8. *Astrophys. J.* **779**, 129. DOI. ADS.

Lemen, J.R., Title, A.M., Akin, D.J., Boerner, P.F., Chou, C., Drake, J.F., Duncan, D.W., Edwards, C.G., Friedlaender, F.M., Heyman, G.F., Hurlburt, N.E., Katz, N.L., Kushner, G.D., Levay, M., Lindgren, R.W., Mathur, D.P., McFeaters, E.L., Mitchell, S., Rehse, R.A., Schrijver, C.J., Springer, L.A., Stern, R.A., Tarbell, T.D., Wuelser, J.-P., Wolfson, C.J., Yanari, C., Bookbinder, J.A., Cheimets, P.N., Caldwell, D., Deluca, E.E., Gates, R.,

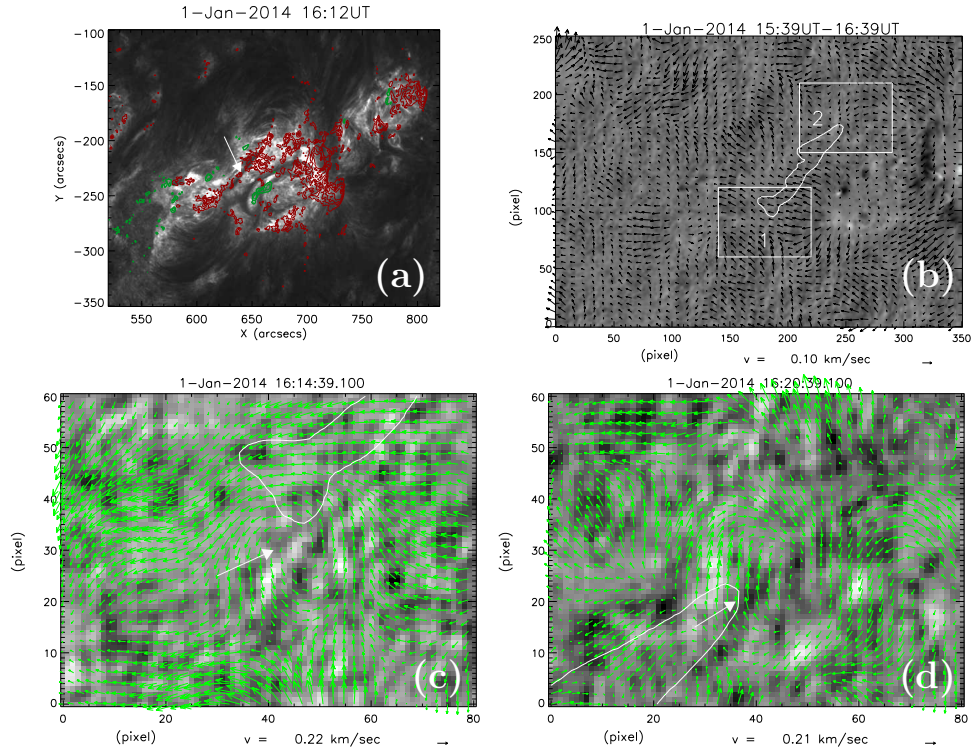

Figure 9. Same as Fig. 7, but for event 7.

Golub, L., Park, S., Podgorski, W.A., Bush, R.I., Scherrer, P.H., Gummin, M.A., Smith, P., Auker, G., Jerram, P., Pool, P., Soufli, R., Windt, D.L., Beardsley, S., Clapp, M., Lang, J., Waltham, N.: 2012, The Atmospheric Imaging Assembly (AIA) on the Solar Dynamics Observatory (SDO). *Solar Phys.* **275**, 17. DOI. ADS.

Li, X., Morgan, H., Leonard, D., Jeska, L.: 2012, A Solar Tornado Observed by AIA/SDO: Rotational Flow and Evolution of Magnetic Helicity in a Prominence and Cavity. *Astrophys. J. Lett.* **752**, L22. DOI. ADS.

Liggett, M., Zirin, H.: 1984, Rotation in prominences. *Solar Phys.* **91**, 259. DOI. ADS.

Liu, C., Lee, J., Yurchyshyn, V., Deng, N., Cho, K.-s., Karlický, M., Wang, H.: 2007, The Eruption from a Sigmoidal Solar Active Region on 2005 May 13. *Astrophys. J.* **669**, 1372. DOI. ADS.

Liu, W., Wang, T.-J., Dennis, B.R., Holman, G.D.: 2009, Episodic X-Ray Emission Accompanying the Activation of an Eruptive Prominence: Evidence of Episodic Magnetic Reconnection. *Astrophys. J.* **698**, 632. DOI. ADS.

Mackay, D.H., Karpen, J.T., Ballester, J.L., Schmieder, B., Aulanier, G.: 2010, Physics of solar prominences: II – magnetic structure and dynamics. *Space Sci. Rev.* **151**, 333. DOI. ADS.

Manchester, W. IV, Gombosi, T., DeZeeuw, D., Fan, Y.: 2004, Eruption of a Buoyantly Emerging Magnetic Flux Rope. *Astrophys. J.* **610**, 588. DOI. ADS.

Martin, S.F.: 1998, Conditions for the Formation and Maintenance of Filaments (Invited Review). *Solar Phys.* **182**, 107. DOI. ADS.

Martin, S.F.: 2003, Signs of helicity in solar prominences and related features. *Adv. Space Res.* **32**, 1883. DOI. ADS.

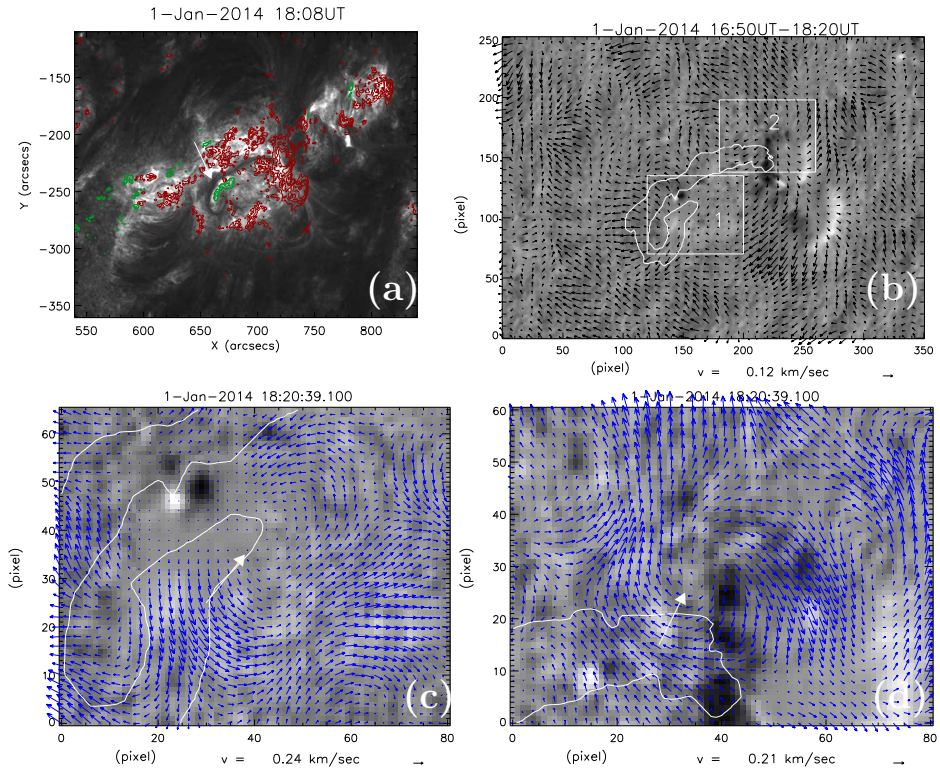

Figure 10. Same as Fig. 7, but for event 8.

November, L.J., Simon, G.W.: 1988, Precise proper-motion measurement of solar granulation. *Astrophys. J.* **333**, 427. DOI. ADS.

Panasenco, O., Martin, S.F.: 2008, Topological Analyses of Symmetric Eruptive Prominences. In: Howe, R., Komm, R.W., Balasubramaniam, K.S., Petrie, G.J.D. (eds.) *Subsurface and Atmospheric Influences on Solar Activity*, *Astronomical Society of the Pacific Conference Series* **383**, 243. ADS.

Panasenco, O., Martin, S., Joshi, A.D., Srivastava, N.: 2011, Rolling motion in erupting prominences observed by STEREO. *Journal of Atmospheric and Solar-Terrestrial Physics* **73**, 1129. DOI. ADS.

Panasenco, O., Martin, S.F., Velli, M., Vourlidas, A.: 2013, Origins of Rolling, Twisting, and Non-radial Propagation of Eruptive Solar Events. *Solar Phys.* **287**, 391. DOI. ADS.

Panesar, N.K., Innes, D.E., Tiwari, S.K., Low, B.C.: 2013, A solar tornado triggered by flares? *Astron. Astrophys.* **549**, A105. DOI. ADS.

Parker, E.N.: 1974, The Dynamical Properties of Twisted Ropes of Magnetic Field and the Vigor of New Active Regions on the Sun. *Astrophys. J.* **191**, 245. DOI. ADS.

Pesnell, W.D., Thompson, B.J., Chamberlin, P.C.: 2012, The Solar Dynamics Observatory (SDO). *Solar Phys.* **275**, 3. DOI. ADS.

Ravindra, B.: 2006, Moving Magnetic Features in and out of Penumbral Filaments. *Solar Phys.* **237**, 297. DOI. ADS.

Rust, D.M.: 2003, The helicial flux rope structure of solar filaments. *Advances in Space Research* **32**, 1895. DOI. ADS.

Rust, D.M., LaBonte, B.J.: 2005, Observational Evidence of the Kink Instability in Solar Filament Eruptions and Sigmoids. *Astrophys. J. Lett.* **622**, L69. DOI. ADS.

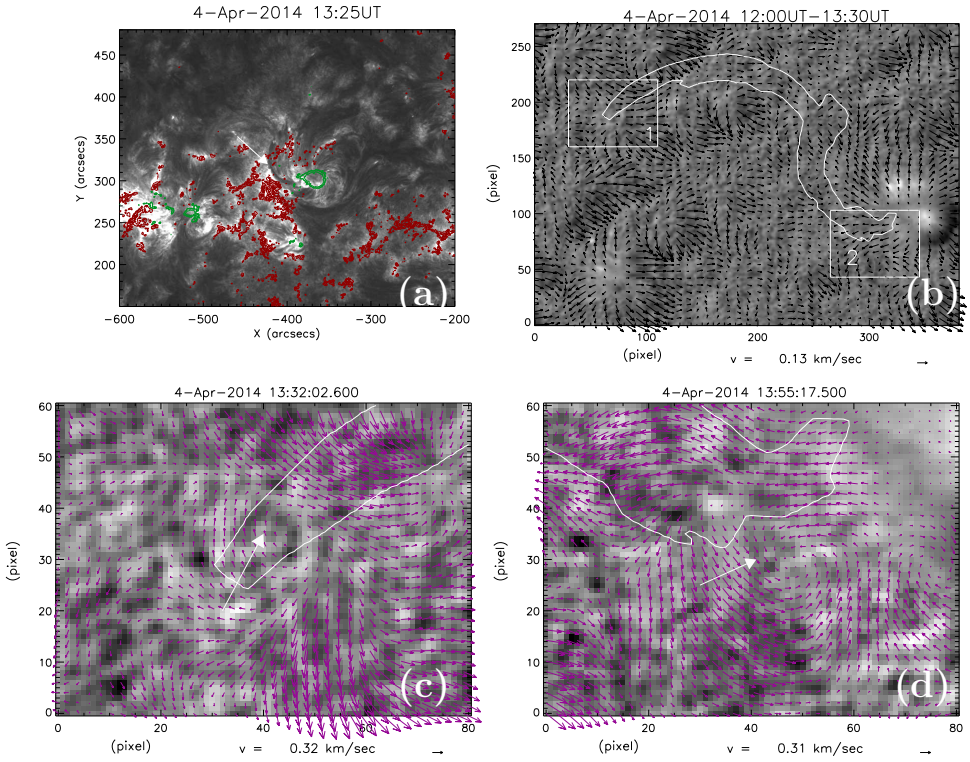

Figure 11. Same as Fig. 7, but for event 9.

Sakurai, K.: 1976, Motion of sunspot magnetic fields and its relation to solar flares. *Solar Phys.* **47**, 261. DOI. ADS.

Scherrer, P.H., Schou, J., Bush, R.I., Kosovichev, A.G., Bogart, R.S., Hoeksema, J.T., Liu, Y., Duvall, T.L., Zhao, J., Title, A.M., Schrijver, C.J., Tarbell, T.D., Tomczyk, S.: 2012, The Helioseismic and Magnetic Imager (HMI) Investigation for the Solar Dynamics Observatory (SDO). *Solar Phys.* **275**, 207. DOI. ADS.

Schou, J., Scherrer, P.H., Bush, R.I., Wachter, R., Couvidat, S., Rabello-Soares, M.C., Bogart, R.S., Hoeksema, J.T., Liu, Y., Duvall, T.L., Akin, D.J., Allard, B.A., Miles, J.W., Rairden, R., Shine, R.A., Tarbell, T.D., Title, A.M., Wolfson, C.J., Elmore, D.F., Norton, A.A., Tomczyk, S.: 2012, Design and Ground Calibration of the Helioseismic and Magnetic Imager (HMI) Instrument on the Solar Dynamics Observatory (SDO). *Solar Phys.* **275**, 229. DOI. ADS.

Su, Y., van Ballegooijen, A.: 2013, Rotating Motions and Modeling of the Erupting Solar Polar-crown Prominence on 2010 December 6. *Astrophys. J.* **764**, 91. DOI. ADS.

Su, Y., Wang, T., Veronig, A., Temmer, M., Gan, W.: 2012, Solar Magnetized "Tornadoes:" Relation to Filaments. *Astrophys. J. Lett.* **756**, L41. DOI. ADS.

Thompson, W.T.: 2011, Strong rotation of an erupting quiescent polar crown prominence. *Journal of Atmospheric and Solar-Terrestrial Physics* **73**, 1138. DOI. ADS.

Titov, V.S., Démoulin, P.: 1999, Basic topology of twisted magnetic configurations in solar flares. *Astron. Astrophys.* **351**, 707. ADS.

Török, T., Kliem, B.: 2005, Confined and Ejective Eruptions of Kink-unstable Flux Ropes. *Astrophys. J. Lett.* **630**, L97. DOI. ADS.

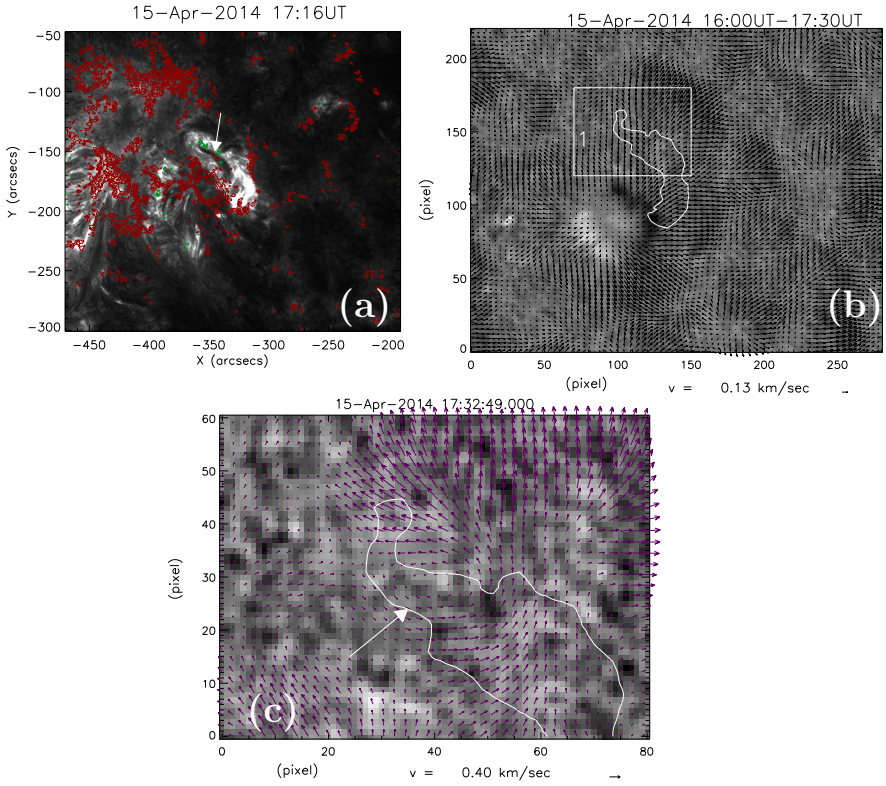

Figure 12. Same as Fig. 7, but for event 10. (c) Rotational velocity pattern observed in the location 1 for this event.

Török, T., Berger, M.A., Kliem, B.: 2010, The writhe of helical structures in the solar corona. *Astron. Astrophys.* **516**, A49. DOI. ADS.

Török, T., Kliem, B., Berger, M.A., Linton, M.G., Démoulin, P., van Driel-Gesztelyi, L.: 2014, The evolution of writhe in kink-unstable flux ropes and erupting filaments. *Plasma Physics and Controlled Fusion* **56**(6), 064012. DOI. ADS.

van Ballegooijen, A.A.: 2004, Observations and Modeling of a Filament on the Sun. *Astrophys. J.* **612**, 519. DOI. ADS.

Wang, Y.-M., Muglach, K., Kliem, B.: 2009, Endpoint Brightenings in Erupting Filaments. *Astrophys. J.* **699**, 133. DOI. ADS.

Wedemeyer, S., Scullion, E., Rouppe van der Voort, L., Bosnjak, A., Antolin, P.: 2013, Are Giant Tornadoes the Legs of Solar Prominences? *Astrophys. J.* **774**, 123. DOI. ADS.

Welsch, B.T., Fisher, G.H., Abbett, W.P., Regnier, S.: 2004, ILCT: Recovering Photospheric Velocities from Magnetograms by Combining the Induction Equation with Local Correlation Tracking. *Astrophys. J.* **610**, 1148. DOI. ADS.

Williams, D.R., Török, T., Démoulin, P., van Driel-Gesztelyi, L., Kliem, B.: 2005, Eruption of a Kink-unstable Filament in NOAA Active Region 10696. *Astrophys. J. Lett.* **628**, L163. DOI. ADS.

Zhou, G.P., Wang, J.X., Zhang, J., Chen, P.F., Ji, H.S., Dere, K.: 2006, Two Successive Coronal Mass Ejections Driven by the Kink and Drainage Instabilities of an Eruptive Prominence. *Astrophys. J.* **651**, 1238. DOI. ADS.

Zirker, J.B., Engvold, O., Martin, S.F.: 1998, Counter-streaming gas flows in solar prominences as evidence for vertical magnetic fields. *Nature* **396**, 440. DOI. ADS.

Zuccarello, F.P., Seaton, D.B., Mierla, M., Poedts, S., Rachmeler, L.A., Romano, P., Zuccarello, F.: 2014, Observational Evidence of Torus Instability as Trigger Mechanism for Coronal Mass Ejections: The 2011 August 4 Filament Eruption. *Astrophys. J.* **785**, 88. DOI. ADS.